Unfolded Proteins Are Ire1-Activating Ligands That Directly Induce the Unfolded Protein Response

Brooke M. Gardner, *et al.*

Science **333**, 1891 (2011);
DOI: 10.1126/science.1209126

evolution produced GEX-GECO1 (table S1 and figs. S2 and S4D), which exhibits a 2600% change in excitation ratio, a K_d of 318 nM, and the most rapid approach to equilibrium (k_{obs}) of any of the GECOs (table S3 and fig. S7).

To explore the utility of our best GECOs, we performed a series of imaging experiments to investigate their performance relative to previously reported indicators and to determine whether they could be used for multicolor Ca^{2+} imaging in single cells. Initially, we expressed individual GECOs in HeLa cells and imaged their intensity (or ratio) during treatment with histamine and in situ dynamic range calibration (table S4 and Fig. 3, A to H). The performance of the GECOs in cells closely paralleled their performance in vitro. We next explored the use of the G- and R-GECO1 in dissociated rat hippocampal neurons (Fig. 3, I and J). Consistent with our HeLa experiments, G-GECO1 proved superior to, and R-GECO1 comparable to, GCaMP3 for imaging of spontaneous Ca^{2+} oscillations. To achieve imaging of neuronal activity in a whole animal, we turned to GEM-GECO1 because of its large ratiometric change. Exposure of a transgenic *Caenorhabditis elegans*, with GEM-GECO1 expressed in the AWA sensory neuron, to a perfused solution of diacetyl produced a 44% ratio change (Fig. 3, K and L), a substantial improvement over the 18% ratio change obtained with YC3.60 under similar conditions (*13*). This improvement was obtained with a cyan FP–yellow FP (CFP-YFP) filter set that provided diminished autofluorescence signal but is not ideally matched to the GEM-GECO1 spectrum.

The palette of GECOs transforms Ca^{2+} imaging from a monochromatic to a multichromatic endeavor. With appropriate targeting and selection of GECO hues, it should be possible to visualize correlated changes in Ca^{2+} in different organelles of a single cell. To explore this possibility, we imaged HeLa cells cotransfected with plasmids encoding targeted versions of R-GECO1, G-GECO1, and either B-GECO1 or GEM-GECO1 (Fig. 4, A to E). As mitochondrial autofluorescence interferes with the emission of B-GECO1, but not with the ratiometric emission of GEM-GECO1, we prefer the latter three-color combination. To determine whether R-GECO1 could be used to image Ca^{2+} dynamics in conjunction with a CFP-YFP FRET-based indicator, we coexpressed R-GECO1 and ATeam1.03, a FRET-based adenosine 5′-triphosphate (ATP) indicator (*14*), in HeLa cells. As recently observed with a synthetic Ca^{2+} indicator (*15*), histamine treatment resulted in transient increases in cytoplasmic (Fig. 4F) and mitochondrial (Fig. 4G) ATP concentrations, albeit with a lag relative to cytoplasmic Ca^{2+}.

In summary, we have engineered a palette of GECOs and have demonstrated that they open the door to Ca^{2+} imaging experiments that were previously impractical. Specifically, these indicators enable imaging of multiple Ca^{2+} indicators in single cells; imaging of neuronal activity in *C. elegans* with improved sensitivity; and, in the case of R-GECO1, multiparameter imaging with CFP-YFP FRET-based biosensors. In addition, GEM-GECO1 and R-GECO1 should facilitate imaging of neuronal activity after optogenetic channel activation, because they are excited at wavelengths spectrally distinct from the action spectra of certain channels (*16*).

References and Notes

1. R. Y. Tsien, in *Calcium as a Cellular Regulator*, E. Carafoli and C. B. Klee, Eds. (Oxford Univ. Press, Oxford, 1999), pp. 28–54.
2. A. Miyawaki *et al.*, *Nature* **388**, 882 (1997).
3. J. Nakai, M. Ohkura, K. Imoto, *Nat. Biotechnol.* **19**, 137 (2001).
4. T. Nagai, A. Sawano, E. S. Park, A. Miyawaki, *Proc. Natl. Acad. Sci. U.S.A.* **98**, 3197 (2001).
5. Single-letter abbreviations for amino acid residues are: A, Ala; C, Cys; D, Asp; E, Glu; F, Phe; G, Gly; H, His; I, Ile; K, Lys; L, Leu; M, Met; N, Asn; P, Pro; Q, Gln; R, Arg; S, Ser; T, Thr; V, Val; W, Trp; and Y, Tyr.
6. Q. Wang, B. Shui, M. I. Kotlikoff, H. Sondermann, *Structure* **16**, 1817 (2008).
7. J. Akerboom *et al.*, *J. Biol. Chem.* **284**, 6455 (2009).
8. Y. N. Tallini *et al.*, *Proc. Natl. Acad. Sci. U.S.A.* **103**, 4753 (2006).
9. L. Tian *et al.*, *Nat. Methods* **6**, 875 (2009).
10. Materials and methods are available as supporting material on *Science* Online.
11. N. C. Shaner *et al.*, *Nat. Methods* **5**, 545 (2008).
12. H. Zhao, W. Zha, *Nat. Protoc.* **1**, 1865 (2006).
13. Y. Shinkai *et al.*, *J. Neurosci.* **31**, 3007 (2011).
14. H. Imamura *et al.*, *Proc. Natl. Acad. Sci. U.S.A.* **106**, 15651 (2009).
15. M. Nakano, H. Imamura, T. Nagai, H. Noji, *ACS Chem. Biol.* **6**, 709 (2011).
16. F. Zhang *et al.*, *Nat. Protoc.* **5**, 439 (2010).
17. C. M. Barrett, N. Ray, J. D. Thomas, C. Robinson, A. Bolhuis, *Biochem. Biophys. Res. Commun.* **304**, 279 (2003).

Acknowledgments: We thank L. L. Looger for GCaMP3 cDNA (Addgene plasmid 22692) and H. Imamura for AT1.03 and mitAT1.03 plasmids. Technical advice or support was provided by J. H. Weiner, Q. Tran, K. Saito, T. Matsuda, N. Sato, N. Yonezawa, the Nikon Imaging Center at Hokkaido University, and the University of Alberta Molecular Biology Service Unit. Sequences have been deposited in GenBank (accession nos. JN258409 to JN258415). Plasmid requests will be handled through Addgene and covered under the Uniform Biological Material Transfer Agreement. This work was supported by Alberta Innovates (Y.Z.); Japan society for the Promotion of Science (JSPS), Canadian Institutes of Health Research, and Natural Sciences and Engineering Research Council of Canada (R.E.C.); Ministry of Education, Culture, Sports, Science, and Technology of Japan Grants in Aid for Scientific Research (KAKENHI) 20115003 and 22150003 (T.I.); and PRESTO from the Japan Science and Technology Agency and FIRST from JSPS (T.N.). R.E.C. holds a Tier II Canada Research Chair in Bioanalytical Chemistry.

Supporting Online Material

www.sciencemag.org/cgi/content/full/science.1208592/DC1
Materials and Methods
SOM Text
Figs. S1 to S9
Tables S1 to S6
Movie S1
References (*18*–*24*)

18 May 2011; accepted 17 August 2011
Published online 8 September 2011;
10.1126/science.1208592

Unfolded Proteins Are Ire1-Activating Ligands That Directly Induce the Unfolded Protein Response

Brooke M. Gardner[1] and Peter Walter[1,2]*

The unfolded protein response (UPR) detects the accumulation of unfolded proteins in the endoplasmic reticulum (ER) and adjusts the protein-folding capacity to the needs of the cell. Under conditions of ER stress, the transmembrane protein Ire1 oligomerizes to activate its cytoplasmic kinase and ribonuclease domains. It is unclear what feature of ER stress Ire1 detects. We found that the core ER-lumenal domain (cLD) of yeast Ire1 binds to unfolded proteins in yeast cells and to peptides primarily composed of basic and hydrophobic residues in vitro. Mutation of amino acid side chains exposed in a putative peptide-binding groove of Ire1 cLD impaired peptide binding. Peptide binding caused Ire1 cLD oligomerization in vitro, suggesting that direct binding to unfolded proteins activates the UPR.

Secretory and transmembrane proteins fold within the endoplasmic reticulum (ER). Contingent on proper folding, they are either exported to the Golgi apparatus or degraded. An accumulation of unfolded proteins activates the unfolded protein response (UPR), a transcriptional program that restores ER protein-folding homeostasis (*1*). The transmembrane protein Ire1 induces the UPR by oligomerizing. Oligomerization activates Ire1's cytoplasmic kinase and ribonuclease (RNase) domains and initiates a nonconventional mRNA splicing reaction of *HAC1* mRNA. Spliced *HAC1* mRNA is translated to produce the transcription factor Hac1, which up-regulates protein-folding

[1]Department of Biochemistry and Biophysics, University of California, San Francisco, San Francisco, CA 94158, USA. [2]Howard Hughes Medical Institute, University of California, San Francisco, San Francisco, CA 94158, USA.

*To whom correspondence should be addressed. E-mail: peter@walterlab.ucsf.edu

machinery (*2*–*4*). The mechanism of Ire1 activation and signal transduction is conserved from yeast to mammals (*5*–*9*); however, it is unclear how Ire1 senses ER stress.

A direct binding model, in which Ire1 binding to unfolded proteins causes its oligomerization, is suggested by structural studies on the conserved core of yeast Ire1 ER-lumenal domain (cLD). The cLD structure contains two interfaces: Interface 1 creates a twofold symmetric dimer containing a deep groove, whereas interface 2 permits further oligomerization (fig. S1) (*10*). Mutation of either interface diminishes oligomerization and decreases *HAC1* mRNA splicing (*11*). The groove formed across interface 1 has architectural similarity to the peptide-binding groove of major histocompatibility complex I (MHCI), suggesting that Ire1 binds to unfolded proteins and that binding increases Ire1 oligomerization (*10*). Also, purified Ire1 cLD prevents the aggregation of unfolded proteins (*12*), suggesting that it binds exposed, aggregation-prone regions.

An alternative model poses that BiP, a predominant ER-resident Hsp70 chaperone that associates with inactive Ire1, detects ER stress by preferentially binding to accumulating unfolded proteins and releasing Ire1 for oligomerization (*13*, *14*). In yeast, however, BiP release cannot be the primary activation step because mutations in Ire1 that impair BiP binding still properly respond to ER stress (*10*, *15*, *16*).

To test the hypothesis that unfolded proteins are Ire1-activating ligands, we determined whether Ire1 interacts with a constitutively misfolded mutant (G255R) of carboxypeptidase Y [wild type (WT), CPY; mutant, CPY*] that is retained in the ER (*17*, *18*). Expression of CPY* induced

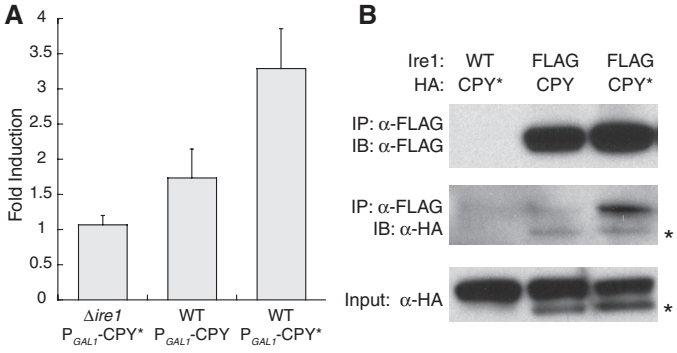

Fig. 1. An unfolded protein coimmunoprecipitates with Ire1. (**A**) The UPR activated by inducible CPY/CPY*-HA was measured with a 4×UPRE-GFP (unfolded protein response element–green fluorescent protein) reporter. Fold induction is the ratio of median fluorescein isothiocyanate (FITC) intensity of cells in 2% galactose to cells in 2% raffinose after 4 hours. Error bars are SD; $n \geq 4$ biological replicates. (**B**) FLAG-tagged Ire1 was immunoprecipitated from cells expressing CPY-HA or CPY*-HA (2 hours, 2% galactose); CPY/CPY*-HA was detected with antibody to HA. The asterisk indicates unglycosylated CPY/CPY*. IP, immunoprecipitation; IB, immunoblot.

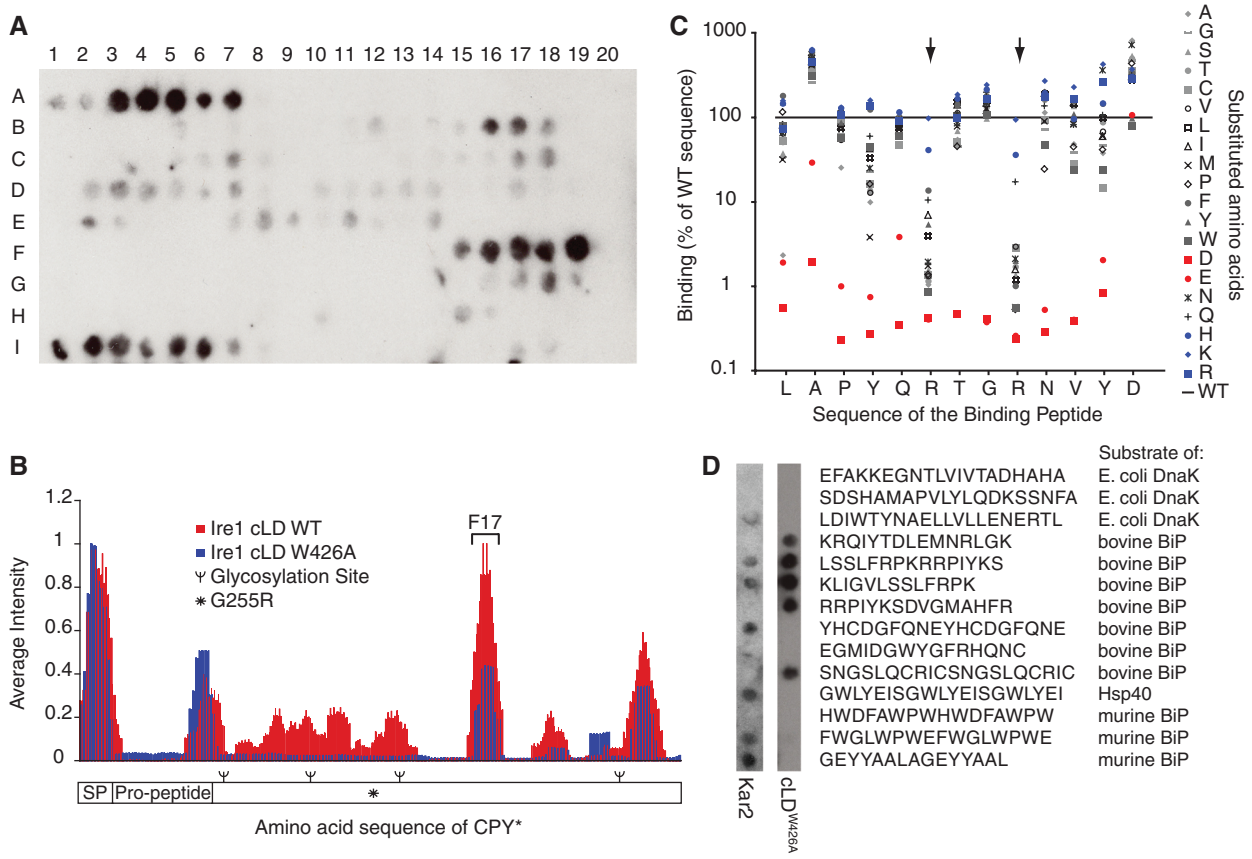

Fig. 2. Ire1 binds specific regions in CPY* containing basic and hydrophobic residues. (**A**) Binding of 500 nM GST-cLD to a peptide array tiling along the sequence of CPY* was detected with antibody to GST. (**B**) The contribution of each amino acid in CPY*'s sequence to Ire1-cLD binding (WT and W426A) was calculated by averaging the intensity of spots containing that amino acid (*19*). Values were plotted along the sequence of CPY*. SP, signal peptide. (**C**) An array composed of peptides with single amino acid substitutions in peptide F17 from the CPY* tiling array (AQLAPYQRTGRNVYD) was probed with GST-cLD^{W426A} and GST-cLD (fig. S3). The binding intensity of the mutated peptides was normalized to the intensity of the wild-type peptide. Large arrows highlight the basic residues in F17. Blue indicates introduced basic residues. Red indicates introduced acidic residues. (**D**) A peptide array of chaperone substrates shows that GST-cLD^{W426A} and Kar2 bind a different subset of peptides.

the UPR in an Ire1-dependent manner, whereas expression of wild-type CPY induced the UPR to a lesser extent (Fig. 1A). To assess whether UPR induction correlated with binding to Ire1, we immunoprecipitated FLAG-tagged Ire1 from cells expressing hemagglutinin (HA)–tagged CPY or CPY* at equivalent amounts. CPY*-HA coimmunoprecipitated with Ire1 in larger amounts than did CPY-HA (Fig. 1B), mirroring the UPR-induction efficiency of each protein (*19*).

To show that Ire1 can bind directly to CPY* and identify binding sites, we probed an array of peptide sequences derived from tiling along the sequence of CPY* with purified cLD tagged with glutathione *S*-transferase (GST) (Fig. 2A). To compare GST-cLD binding between arrays and across CPY*'s sequence, we quantified the average signal intensity attributed to each amino acid in CPY* (Fig. 2B). GST-cLD bound to the signal peptide, propeptide, and C-terminal regions of CPY*. The GST tag did not contribute to binding because GST alone did not bind to the array. GST-cLD did not bind strongly to the region containing the G255R mutation, suggesting that this mutation exposes other sites through large-scale misfolding. A mutant of GST-cLD—W426A, which disrupts interface 2 but preserves the putative peptide-binding groove (*10*, *11*)—bound to similar peptides on the array as GST-cLD (Fig. 2B). The lowered affinity of GST-cLD^{W426A} to regions of weak binding by wild-type GST-cLD is likely due to reduced avidity in the absence of higher-order oligomers.

The regions of CPY* that GST-cLD (WT and W426A) recognized did not reveal a consensus sequence. However, comparison of the amino acid composition of binding peptides with that of CPY/CPY* showed a strong preference for arginine and an exclusion of acidic amino acids. Leucine and phenylalanine were also enriched in the binding peptides (fig. S2). Further analysis by means of systematic mutation of a binding peptide (derived from spot F17 in Fig. 2A) confirmed the bias for basic residues (Fig. 2C). Mutation of either of the two arginines—and to a lesser extent the two tyrosines—in the binding peptide to nonbasic amino acids reduced binding of GST-cLD (W426A and WT) (Fig. 2C and fig. S3). Similarly, mutation of any amino acid to an acidic residue lowered the affinity of GST-cLD^{W426A} for the peptide (Fig. 2C).

The Hsp70 family of chaperones, which includes BiP (Kar2 in yeast), also binds regions containing basic and hydrophobic residues (*20*–*23*). The overlap between Hsp70 and Ire1 substrates is not congruent, however, because Ire1 GST-cLD^{W426A} did not bind measurably to several control peptides derived from known DnaK and BiP substrates (Fig. 2D). Furthermore, probing the same peptides with purified Kar2 showed that Kar2 and Ire1 bound an overlapping, but not identical, subset of peptides (Fig. 2D).

To determine the affinity of Ire1 cLD for peptides, we measured their binding to cLD^{W426A} by means of fluorescence anisotropy. CPY*-derived peptide FAM-F17 bound with an affinity of $K_{1/2}$ = 172 μM (Fig. 3A) and a Hill coefficient of 1.4. When a fragment of CPY containing this region was expressed within the ER, it induced the UPR and coimmunoprecipitated with Ire1 (fig. S4). A signal peptide, ΔEspP-FAM, which contains hydrophobic and basic amino acids as preferred by Ire1 (*24*), bound to Ire1 cLD^{W426A} with higher affinity ($K_{1/2}$ = 0.75 μM, Hill coefficient = 1.2). Although signal peptides are not normally displayed in the ER lumen, ΔEspP proved a useful tool with which to probe peptide/cLD interactions (Fig. 3A). Mutational analysis of ΔEspP on a peptide array confirmed that Ire1 cLD^{W426A} bound ΔEspP with the same preference for basic and hydrophobic residues and intolerance of acidic residues (fig. S5).

These $K_{1/2}$s are composites of several equilibria: Ire1 cLD self-association and binding of Ire1 cLD monomer and dimer to peptide. The lack of Ire1 cLD monomer bound to peptide (Fig. 4B) and the Hill coefficient greater than 1 in the anisotropy assay suggest that Ire1 binds the peptides in a cooperative manner. By modeling Ire1 binding to peptide as a cooperative reaction in which there is little Ire1 monomer bound to peptide (Fig. 4B), we estimate the affinity of Ire1 dimer for ΔEspP-FAM is 0.068 μM (fig. S6).

To determine whether residues in the groove are important for peptide binding, we tested the mutant M229A-F265A-Y301A (ΔMFY), which changes three hydrophobic residues along the floor of the groove to alanines and reduces UPR signaling in vivo (*10*). We observed that cLD-ΔMFY bound ΔEspP-FAM with reduced affinity ($K_{1/2}$ = 42 ± 2 μM) (Fig. 3D), corresponding with reduced UPR signaling (Fig. 3B) and impaired survival upon UPR-induction (fig. S7). Thus, Ire1 binding with high affinity to ΔEspP-FAM depends on groove residues.

To interrogate whether cLD oligomerizes in response to peptide binding, as hypothesized by the direct binding model, we assessed the oligomeric state of cLD bound to ΔEspP. Velocity sedimentation of wild-type cLD showed a distribution of monomer, dimer, and tetramer species when assessed without peptide and a shift toward heterogeneous larger oligomers in the presence of ΔEspP (Fig. 4A). To limit peptide-induced oligomerization to more discrete species, we repeated this experiment with Ire1 cLD^{W426A} and observed only two predominant species of Ire1 cLD^{W426A} corresponding to monomer and dimer (Fig. 4B). Addition of ΔEspP caused Ire1 cLD^{W426A} to dimerize completely (Fig. 4B). In agreement, sedimentation equilibrium showed a shift from the simulated monomer toward the simulated dimer (Fig. 4C). By fitting the data

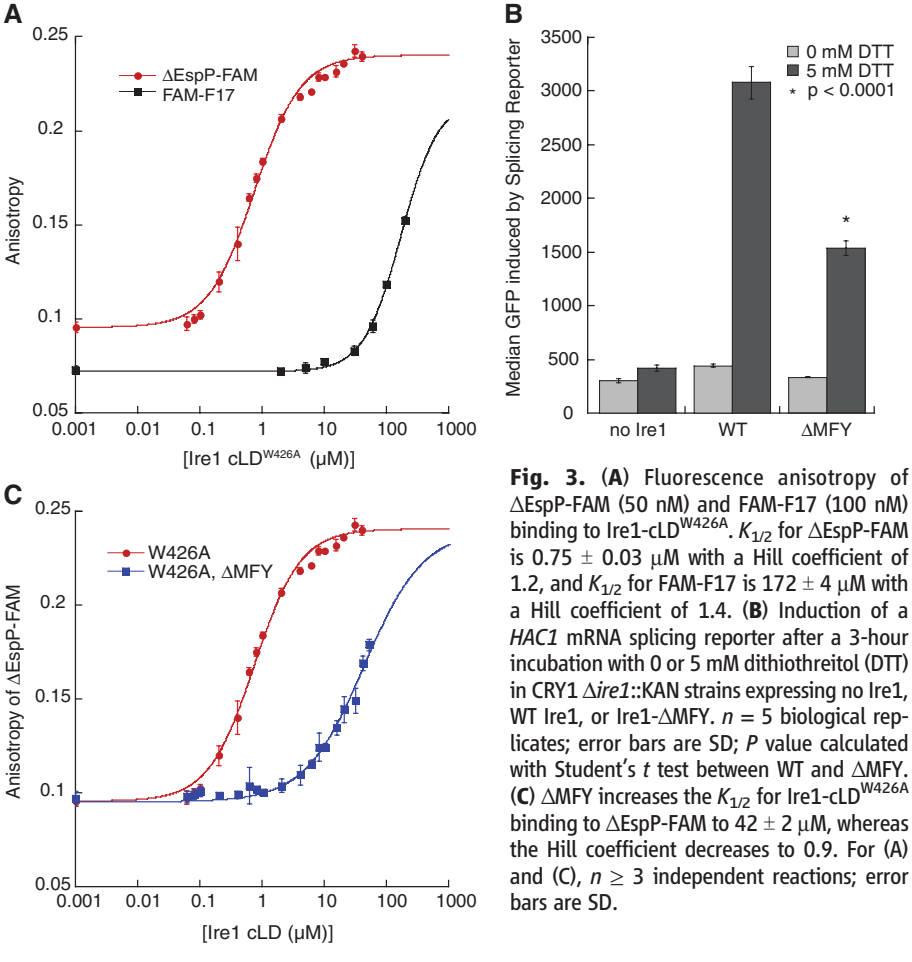

Fig. 3. (**A**) Fluorescence anisotropy of ΔEspP-FAM (50 nM) and FAM-F17 (100 nM) binding to Ire1-cLD^{W426A}. $K_{1/2}$ for ΔEspP-FAM is 0.75 ± 0.03 μM with a Hill coefficient of 1.2, and $K_{1/2}$ for FAM-F17 is 172 ± 4 μM with a Hill coefficient of 1.4. (**B**) Induction of a *HAC1* mRNA splicing reporter after a 3-hour incubation with 0 or 5 mM dithiothreitol (DTT) in CRY1 Δ*ire1*::KAN strains expressing no Ire1, WT Ire1, or Ire1-ΔMFY. n = 5 biological replicates; error bars are SD; P value calculated with Student's t test between WT and ΔMFY. (**C**) ΔMFY increases the $K_{1/2}$ for Ire1-cLD^{W426A} binding to ΔEspP-FAM to 42 ± 2 μM, whereas the Hill coefficient decreases to 0.9. For (A) and (C), $n \geq 3$ independent reactions; error bars are SD.

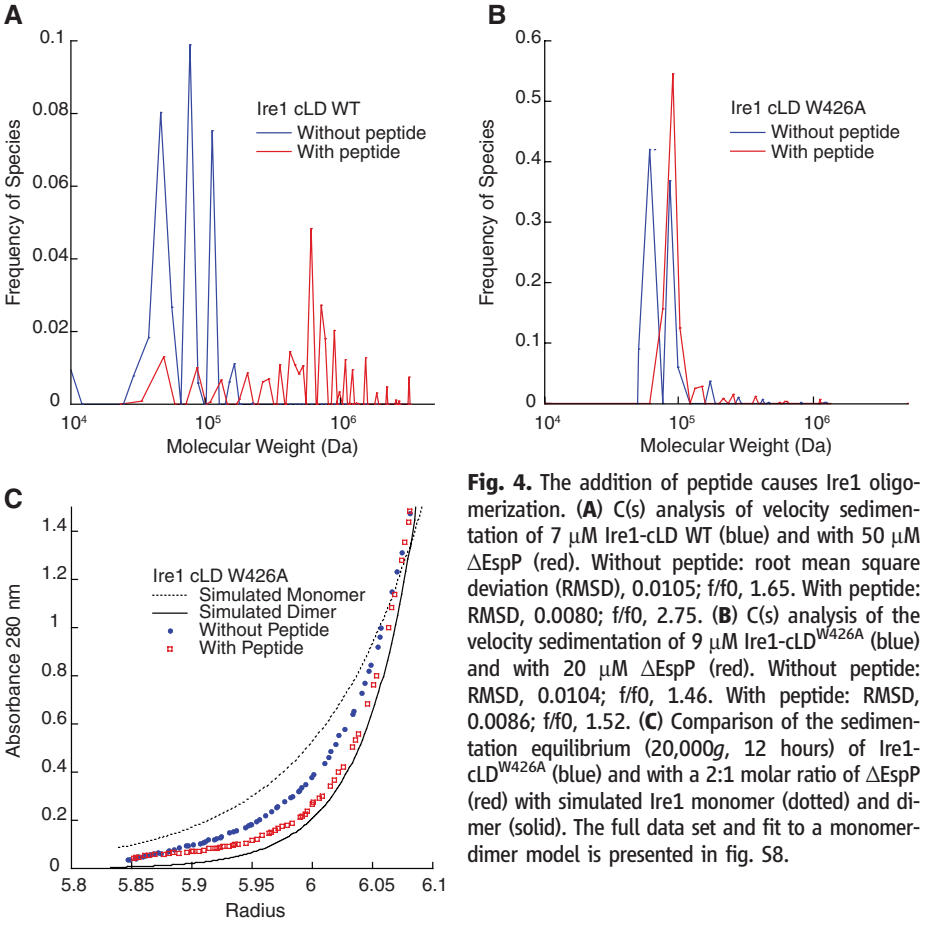

Fig. 4. The addition of peptide causes Ire1 oligomerization. (**A**) C(s) analysis of velocity sedimentation of 7 μM Ire1-cLD WT (blue) and with 50 μM ΔEspP (red). Without peptide: root mean square deviation (RMSD), 0.0105; f/f0, 1.65. With peptide: RMSD, 0.0080; f/f0, 2.75. (**B**) C(s) analysis of the velocity sedimentation of 9 μM Ire1-cLD^{W426A} (blue) and with 20 μM ΔEspP (red). Without peptide: RMSD, 0.0104; f/f0, 1.46. With peptide: RMSD, 0.0086; f/f0, 1.52. (**C**) Comparison of the sedimentation equilibrium (20,000*g*, 12 hours) of Ire1-cLD^{W426A} (blue) and with a 2:1 molar ratio of ΔEspP (red) with simulated Ire1 monomer (dotted) and dimer (solid). The full data set and fit to a monomer-dimer model is presented in fig. S8.

with a monomer-dimer model, we determined that the dissociation constant (K_d) of Ire1 association without peptide was 8.2 μM (fig. S8). The K_d with peptide could not be determined because there was no remaining Ire1 monomer population; however, the average molecular weight of the species in solution shifted from 62 kD to 88 kD.

Taken together, Ire1cLD binding to peptides causes it to oligomerize, as we predict occurs in cells when Ire1 binds to unfolded proteins. Furthermore, Ire1 coimmunoprecipitated with CPY*. This interaction was recently shown to be impaired by the ΔMFY mutation but not the W426A mutation (*25*), which is consistent with our in vitro work. Because BiP dissociation from Ire1 during ER stress has been ruled out as the primary switch that governs the UPR, we suggest that BiP association fine-tunes Ire1 signaling (*10*, *15*, *16*), whereas unfolded proteins are activating ligands. The lack of congruity between Ire1 and BiP substrates suggests that Ire1 does not always compete with BiP for binding sites and is not dependent on BiP saturation.

Ire1's preference for basic and hydrophobic residues and intolerance of acidic residues was maintained despite the wide range in affinity between the peptides analyzed here. In vivo, where the substrates are unfolded proteins rather than short peptides, this sequence selectivity must be accompanied by selecting for stretches of misfolded proteins that are sufficiently exposed to sample the depth of the groove. Importantly, acidic features prominent in many ER resident proteins, such as ER-retention signals, would render them invisible to Ire1 even if unstructured and exposed.

By sequence, Ire1cLD is conserved from yeast to mammalian Ire1α/Ire1ß, and including the additional metazoan ER-stress sensor PERK (protein kinase RNA-like endoplasmic reticulum kinase). This evolutionary conservation and the central importance of unfolded protein recognition by all of these sensors strongly suggest that these molecules deploy similar mechanisms. However, unlike yeast Ire1, the crystal structure of human Ire1α displays a groove too narrow for peptide binding (*26*). These two static structures can be reconciled if the structure of hIre1 represents a "closed" conformation formed in the absence of bound peptide. In this conformation, interface 2 cannot form, and Ire1 cannot oligomerize. Peptide binding would induce a conformational switch toward an "open" conformation, represented by the yeast Ire1 structure, establishing interface 2 oligomerization and leading to Ire1 activation. In this way, the conformational change is induced through peptide binding, forming the core module of the signaling machine that senses ER stress. The peptide-binding groove and oligomerization interfaces are attractive candidates for targeted drug design that could help alleviate the misregulation of hIre1 and PERK apparent in disease.

References and Notes

1. D. Ron, P. Walter, *Nat. Rev. Mol. Cell Biol.* **8**, 519 (2007).
2. J. S. Cox, P. Walter, *Cell* **87**, 391 (1996).
3. C. Sidrauski, P. Walter, *Cell* **90**, 1031 (1997).
4. T. Kawahara, H. Yanagi, T. Yura, K. Mori, *Mol. Biol. Cell* **8**, 1845 (1997).
5. X. Z. Wang *et al.*, *EMBO J.* **17**, 5708 (1998).
6. X. Shen *et al.*, *Cell* **107**, 893 (2001).
7. M. Calfon *et al.*, *Nature* **415**, 92 (2002).
8. H. Li, A. V. Korennykh, S. L. Behrman, P. Walter, *Proc. Natl. Acad. Sci. U.S.A.* **107**, 16113 (2010).
9. W. Tirasophon, A. A. Welihinda, R. J. Kaufman, *Genes Dev.* **12**, 1812 (1998).
10. J. J. Credle, J. S. Finer-Moore, F. R. Papa, R. M. Stroud, P. Walter, *Proc. Natl. Acad. Sci. U.S.A.* **102**, 18773 (2005).
11. T. Aragón *et al.*, *Nature* **457**, 736 (2009).
12. Y. Kimata *et al.*, *J. Cell Biol.* **179**, 75 (2007).
13. A. Bertolotti, Y. Zhang, L. M. Hendershot, H. P. Harding, D. Ron, *Nat. Cell Biol.* **2**, 326 (2000).
14. K. Okamura, Y. Kimata, H. Higashio, A. Tsuru, K. Kohno, *Biochem. Biophys. Res. Commun.* **279**, 445 (2000).
15. D. Pincus *et al.*, *PLoS Biol.* **8**, e1000415 (2010).
16. Y. Kimata, D. Oikawa, Y. Shimizu, Y. Ishiwata-Kimata, K. Kohno, *J. Cell Biol.* **167**, 445 (2004).
17. A. Finger, M. Knop, D. H. Wolf, *Eur. J. Biochem.* **218**, 565 (1993).
18. In the mutants, other amino acids were substituted at certain locations; for example, G255R indicates that glycine at position 255 was replaced by arginine. Single-letter abbreviations for the amino acid residues are as follows: A, Ala; C, Cys; D, Asp; E, Glu; F, Phe; G, Gly; H, His; I, Ile; K, Lys; L, Leu; M, Met; N, Asn; P, Pro; Q, Gln; R, Arg; S, Ser; T, Thr; V, Val; W, Trp; and Y, Tyr.
19. Materials and methods are available as supporting material on *Science* Online.
20. S. Rüdiger, L. Germeroth, J. Schneider-Mergener, B. Bukau, *EMBO J.* **16**, 1501 (1997).
21. A. de Crouy-Chanel, M. Kohiyama, G. Richarme, *J. Biol. Chem.* **271**, 15486 (1996).
22. G. C. Flynn, T. G. Chappell, J. E. Rothman, *Science* **245**, 385 (1989).
23. S. Blond-Elguindi *et al.*, *Cell* **75**, 717 (1993).
24. J. H. Peterson, C. A. Woolhead, H. D. Bernstein, *J. Biol. Chem.* **278**, 46155 (2003).
25. Y. Ishiwata-Kimata *et al.*, *Mol. Biol. Cell.*, published online 20 July 2011 (10.1091/mbc.E11-04-0295).
26. J. Zhou *et al.*, *Proc. Natl. Acad. Sci. U.S.A.* **103**, 14343 (2006).

Acknowledgments: We thank J. Weissman, G. Narlikar, and D. Mullins for insightful comments; S. Neher and A. Korennykh for their invaluable guidance; and the Walter Lab, especially H. Li, E. van Anken, D. Pincus, C. Gallagher, and M. Diaz for their assistance and scientific discussions. Purified Kar2 was a generous gift from J. Brodsky. We are grateful to the Massachussetts Institute of Technology Biopolymers Institute for synthesizing the peptide arrays. B.G. was supported by a National Science Foundation predoctoral fellowship. P.W. is an investigator of the Howard Hughes Medical Institute.

Supporting Online Material

www.sciencemag.org/cgi/content/full/science.1209126/DC1
Materials and Methods
Figs. S1 to S8

31 May 2011; accepted 8 August 2011
Published online 18 August 2011;
10.1126/science.1209126